All-optical transistor action with bistable switching in a photonic crystal cross-waveguide geometry

Mehmet Fatih Yanik and Shanhui Fan

Ginzton Laboratory, Stanford University, Stanford, California 94304

Marin Soljačić and J. D. Joannopoulos

Department of Physics, Massachusetts Institute of Technology, Cambridge, Massachusetts 02139

We demonstrate all-optical switching action in a nonlinear photonic crystal cross-waveguide geometry with instantaneous Kerr nonlinearity, in which the transmission of a signal can be reversibly switched on and off by a control input. Our geometry accomplishes both spatial and spectral separation between the signal and the control in the nonlinear regime. The device occupies a small footprint of a few micrometers squared and requires only a few milliwatts of power at a 10-Gbit/s switching rate by use of Kerr nonlinearity in AlGaAs below half the electronic bandgap. We also show that the switching dynamics, as revealed by both coupled-mode theory and finite-difference time domain simulations, exhibits collective behavior that can be exploited to generate high-contrast logic levels and all-optical memory. © 2003 Optical Society of America

OCIS codes: 130.4310, 190.1450, 230.4110, 230.5750, 130.3750.

Photonic crystals promise dense and large-scale integration of optical information-processing components. It has recently been shown that the use of nonlinearity in photonic crystal microcavities allows the construction of ultracompact all-optical elements that operate with low power requirements and high speed.[1–6] In this Letter we demonstrate an all-optical transistor action in a nonlinear photonic crystal, in which the transmission of a signal can be reversibly switched on or off by a control input with high contrast and low power.

Our design is based on the photonic crystal cross-waveguide geometry (Fig. 1).[7] In the linear regime this geometry allows the intersection of two waveguides without any cross talk between them. The crystal consists of a square lattice of highly dielectric rods ($n = 3.5$) with a radius of $0.2a$ (a is the lattice constant) embedded in air ($n = 1$), and it has a bandgap for TM modes with electric fields parallel to the rod axis. To form the waveguides, a line of rods is removed along either the x or y axis. The intersection consists of a cavity that supports two dipole modes. Each cavity mode is even with respect to one of the waveguide axes and odd with respect to the other. Since the waveguide modes are even with respect to the waveguide axis, each waveguide couples to only the cavity mode with the same symmetry, thus prohibiting any cross talk.

We create a nonlinear optical switch with this geometry by introducing Kerr nonlinearity to the rod at the center of the cavity. We show that this system allows a control in one waveguide to switch the transmission of a signal on or off in another waveguide (Fig. 1) and that there is no energy exchange between the signal and the control, even in the nonlinear regime, which is essential for densely integrated optical circuits. In addition, this structure can be easily configured such that the signal and the control operate at different frequencies, which is beneficial for wavelength division multiplexing. In the structure shown in Fig. 1, for example, we accomplish a spectral separation of the control and the signal by using a cavity with an elliptical dielectric rod, with axis lengths of $0.54a$ and $0.64a$ along the x and y directions, respectively.
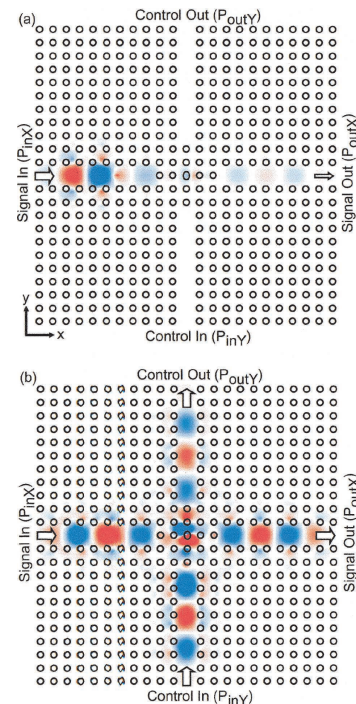

Fig. 1. Electric field distributions in a photonic crystal cross-waveguide switch. (a) Control input $P_{\text{in}Y}$ is absent, and signal output $P_{\text{out}X}$ is low. (b) Control input $P_{\text{in}Y}$ is present, and signal output $P_{\text{out}X}$ is high. The control and signal power are both $\sim$200 mW/μm. Red and blue represent large positive or negative electric fields, respectively. The same color scale is used for both panels. The black circles indicate the positions of the dielectric rods in the photonic crystal.

The dynamic behavior of the system can be described with the following coupled-mode equations:

$$\frac{dS_{\text{out}X}}{dt} = i\omega_X S_{\text{out}X} - i\gamma_X\left(\frac{|S_{\text{out}X}|^2}{P_{XX}} + 2\frac{|S_{\text{out}Y}|^2}{P_{XY}}\right)S_{\text{out}X}$$
$$+ \gamma_X(S_{\text{in}X} - S_{\text{out}X}) - i\gamma_X\frac{S_{\text{out}Y}^2}{P_{XY}}S_{\text{out}X}{}^*,$$

(1)

$$\frac{dS_{\text{out}Y}}{dt} = i\omega_Y S_{\text{out}Y} - i\gamma_Y\left(\frac{|S_{\text{out}Y}|^2}{P_{YY}} + 2\frac{|S_{\text{out}X}|^2}{P_{YX}}\right)S_{\text{out}Y}$$
$$+ \gamma_Y(S_{\text{in}Y} - S_{\text{out}Y}) - i\gamma_Y\frac{S_{\text{out}X}^2}{P_{YX}}S_{\text{out}Y}{}^*.$$

(2)

$S_{\text{in(out)}j}$ is proportional to the field amplitude such that $P_{\text{in(out)}j} = |S_{\text{in(out)}j}|^2$ is the input (output) power in waveguide j. The subscripts X and Y label either the waveguide that is parallel to the x or y axis, respectively, or the cavity mode that couples to the waveguide. $\gamma_j = \omega_j/2Q_j$ is the decay rate for cavity mode j. $P_{ij} = [2\alpha_{ij}(\omega_i/c)^{d-1}n_2 Q_i Q_j]^{-1}$ are the characteristic powers of the system with

$$\alpha_{ij} = \left(\frac{c}{\omega_i}\right)^d \frac{\int_{\text{vol}} d^d r[|\mathbf{E}_i(r)\cdot\mathbf{E}_j(r)|^2 + 2|\mathbf{E}_i(r)\cdot\mathbf{E}_j{}^*(r)|^2]n^2(r)n_2(r)}{[\int_{\text{vol}} d^d r|\mathbf{E}_i(r)|^2 n^2(r)][\int_{\text{vol}} d^d r|\mathbf{E}_j(r)|^2 n^2(r)]n_2(r)_{\text{max}}}, \quad (3)$$

where α is the generalization of the dimensionless scale-invariant nonlinear feedback parameter defined in Ref. 3; here α_{ii} and α_{ij} are the self- and cross-modal overlap factors for the two cavity modes i and j and are obtained from the first-order perturbation theory in terms of the electric fields in the cavity modes $\mathbf{E}_{i(j)}(r) = \frac{1}{2}[\mathbf{E}_{i(j)}(r)\exp(i\omega t) + \mathbf{E}_{i(j)}{}^*(r)\exp(-i\omega t)]$. n_2, ω_j, a, and c are the instantaneous Kerr nonlinearity coefficient, the angular frequency of cavity mode j, the lattice constant of the photonic crystal, and the speed of light, respectively. The last terms on the right-hand side of Eqs. (1) and (2) describe a nonlinear energy exchange process between the control and the signal, which become negligible when the frequencies of the signal and control inputs and the corresponding resonances of the cavity modes are separated by more than the width of the resonances, as in our simulations.

With Eqs. (1) and (2) the general switching behavior of the system can be understood qualitatively as follows: In the absence of the control beam (i.e., $S_{\text{in}Y} = 0$) the signal output versus the signal input exhibits the typical bistable shape in a transmission resonator configuration,[8] as shown with the blue solid curve in Fig. 2. Suppose the signal output level is originally at point A in Fig. 2. Applying a control beam (i.e., nonzero $S_{\text{in}Y}$ and $S_{\text{out}Y}$) shifts the frequency of mode X by an amount that is proportional to $|S_{\text{out}Y}|^2$. The bistable transition threshold of the signal is thus decreased (e.g., the red curve, Fig. 2), resulting in an abrupt transition in the signal output power. Therefore at a given signal input power the control can

stimulate transitions between the bistable states and generate high-contrast logic levels. When the control is turned off, the bistability curve for the signal output moves back to the blue curve, and the signal output drops to the original level at point A. Such reversible switching occurs when the signal input power level lies below the bistable threshold in the absence of the control. For a higher signal input power (for example, point C in Fig. 2) the signal output remains at a higher power level (point E) after the control is turned off, thus exhibiting memory behavior.

Since the transmission of the control is also being modulated by the signal, the detailed switching dynamics is more complicated than in the qualitative discussions presented above. Below we present a rigorous analysis by combining finite-difference time domain (FDTD) simulations with coupled-mode theory. We show that the mutual coupling between the signal and the control can lead to significant improvements in the switching contrast.

We employ the same nonlinear FDTD simulations[9] as in Ref. 5. We choose a Kerr coefficient of $n_2 = 1.5 \times 10^{-17}$ W/m^2, which is achievable with nearly instantaneous nonlinearity in AlGaAs below half the electronic bandgap[10,11] at 1.55 μm. At a low incident power at which the structure behaves linearly we determine that the cavity modes have resonance frequencies of $\omega_X = 0.373(2\pi c/a)$ and $\omega_Y = 0.355(2\pi c/a)$, which fall within the bandgap of the photonic crystal; quality factors of $Q_X = 920$ and $Q_Y = 1005$; and nonlinear modal overlap factors of $\alpha_{XX} = 0.154$, $\alpha_{YY} = 0.172$, $\alpha_{XY} = 0.051$, and $\alpha_{YX} = 0.056$. With these parameters and a lattice constant of $a = 575$ nm the theory predicts characteristic powers of $P_{XX} = 62.75$ mW/μm, $P_{YY} = 49.26$ mW/μm, $P_{XY} = 172.55$ mW/μm, and $P_{YX} = 164.32$ mW/μm.
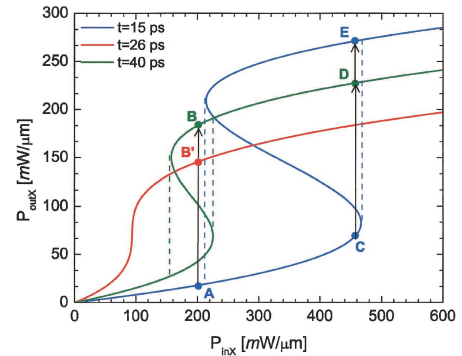

Fig. 2. Input versus output power for the signal in waveguide X, calculated with Eq. (1), with the output power in waveguide Y (and hence the energy in cavity mode Y) kept at constant levels. Blue, red, and green curves correspond to control output powers of 0, 151, and 75 mW/μm, respectively, which is appropriate for various times in the switching process, as shown in Fig. 3.
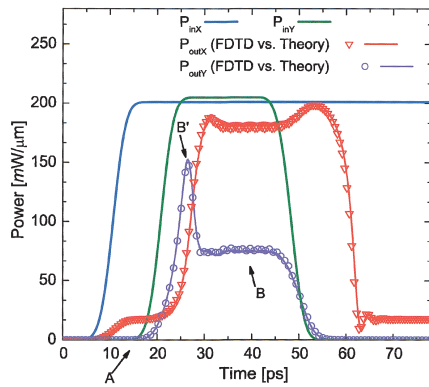
Fig. 3. Input and output power levels for the signal and the control as a function of time. The curves are from coupled-mode theory calculations with Eqs. (1) and (2), and the open circles and triangles are from FDTD simulations. The labels A, B, and B′ indicate the control output power levels that were used to calculate the bistability curves in Fig. 2.

To demonstrate the transistor action, we launch a signal in waveguide X with carrier frequency $\omega_{\mathrm{in}X}$ detuned by $\delta_X \equiv (\omega_X - \omega_{\mathrm{in}X})/\gamma_X = 2\sqrt{3}$ from the resonance of cavity mode X, as shown with the solid blue curve in Fig. 3. ($\delta = \sqrt{3}$ is the minimum detuning threshold for the presence of bistability in the absence of control input.) The power of the input $P_{\mathrm{in}X} = 200$ mW/μm is selected to be below the bistable region in the absence of the control input (point A on the blue curve in Fig. 2). The field pattern of the steady state at $t = 15$ ps is shown in Fig. 1(a). After the steady state has been reached, we launch a control pulse with detuning $\delta_Y \equiv (\omega_Y - \omega_{\mathrm{in}Y})/\gamma_Y = 1.4\sqrt{3}$ and a power of $P_{\mathrm{in}Y} = 205$ mW/μm in waveguide Y, as shown with the green solid curve in Fig. 3. The control switches the signal output to a higher level in approximately 10 ps (point B on the green bistability curve in Fig. 2). The field pattern of the steady state in the presence of the control is shown in Fig. 1(b). Finally, we turn off the control at $t = 45$ ps, and the signal output returns to a low transmission state, completing a reversible switching cycle. There is excellent agreement between our FDTD results and coupled-mode theory with Eqs. (1) and (2).[5]

An interesting feature in Fig. 3 is the presence of a peak in the control output during the initial transient period (labeled as B′). As the control input is switched on, the power in mode Y initially increases, which induces the transition in signal output from point A to point B′ by moving the bistability curve for the signal from the blue curve to the red curve in Fig. 2. In the meantime, however, as the energy increases in the cavity modes, the frequency of mode Y also starts to shift downward, detuning from the control input; eventually reduces its energy from its peak value; and moves the bistability curve for the signal from the red curve to the green curve in Fig. 2. Such collective dynamics can thus be used to generate high contrast in signal output (point B in Fig. 3) with a low power threshold. To ex-

ploit this effect, we have chosen a finite detuning $\delta_Y = 1.4\sqrt{3}$ of the control input from cavity resonance Y.

We note from Eqs. (1) and (2) that the nonlinearity does not mix the signal and control outputs when their frequencies are separated by more than the cavity resonance widths. This is confirmed in the FDTD simulations by analysis of the spectra at the two output ports during the entire switching process.

The structure has a footprint of a few micrometers squared. For 10-Gbit/s applications one could use cavities with in-plane quality factors of approximately $Q_{X(Y)} \simeq 5000$, which are achievable in photonic crystal slabs.[12] Since the bistability power threshold scales as $1/Q^2$, for a three-dimensional structure operating at 1.55 μm with the optical mode confined in the third dimension to a width of approximately half a wavelength, the power requirement is only a few milliwatts and the relative index shift $\delta n/n$ is less than 10^{-3}, which is achievable in materials with instantaneous Kerr nonlinearity. The contrast ratio between the on and off states is approximately 10, and further reduction by orders of magnitude in the power requirement and index shift is achievable by use of smaller detunings $\delta_{X(Y)}$. Finally, the switching is robust against fluctuations in the system parameters and power levels.

References

1. E. Centeno and D. Felbacq, Phys. Rev. B **62,** R7683 (2000).
2. S. F. Mingaleev and Y. S. Kivshar, J. Opt. Soc. Am. B **19,** 2241 (2002).
3. M. Soljacic, M. Ibanescu, S. G. Johnson, Y. Fink, and J. D. Joannopoulos, Phys. Rev. E **66,** 55601 (R) (2002).
4. M. Soljacic, C. Luo, J. D. Joannopoulos, and S. Fan, Opt. Lett. **28,** 637 (2003).
5. M. F. Yanik, S. Fan, and M. Soljacic, Appl. Phys. Lett. **83,** 2739 (2003).
6. S. Scholz, O. Hess, and R. Rühle, Opt. Express **3,** 28 (1998), http://www.opticsexpress.org.
7. S. G. Johnson, C. Manolatou, S. Fan, P. R. Villeneuve, J. D. Joannopoulos, and H. A. Haus, Opt. Lett. **23,** 1855 (1998).
8. H. A. Haus, *Waves and Fields in Optoelectronics* (Prentice-Hall, Englewood Cliffs, N.J., 1984).
9. A. Taflove and S. C. Hagness, *Computational Electrodynamics* (Artech House, Norwood, Mass., 2000).
10. M. N. Islam, C. E. Soccolich, R. E. Slusher, A. F. J. Levi, W. S. Hobson, and M. G. Young, J. Appl. Phys. **71,** 1927 (1992).
11. A. Villeneuve, C. C. Yang, G. I. Stegeman, C. Lin, and H. Lin, J. Appl. Phys. **62,** 2465 (1993).
12. K. Srinivasan and O. Painter, Opt. Express **10,** 670 (2002), http://www.opticsexpress.org.